MSc thesis
Earth, Life and Climate
Universiteit Utrecht

Iron cycling in the Archean as recorded by the Fe isotopes in shales from the Barberton Greenstone Belt

by
NIKLAS STAUSBERG

Supervisors:
DR. PAUL MASON
DR. PIETER VROON
ALEKSANDRA GALIC

Contents

Abstract

The iron cycle on the early earth was significantly different from today due to anoxic oceans and atmosphere. Today, the iron-rich deposits found show proof of this distinct cycle. For a long time, iron formations have been of particular interest because of their economic value and recently, Fe isotopes were used to trace sources and depositional processes. Other sediments from the Precambrian are also distinctively iron-rich and might reflect iron cycling. Here, we present bulk iron isotope measurements of rocks from the Middle Mapepe formation of the Fig-Tree group from the Barb 5 drill core, Barberton Greenstone Belt, South Africa. 42 selected reference samples represent the basin development of the Middle Mapepe from deep anoxic to shallow water settings, including alluvial fans. Iron in the samples was chemically separated from its matrix and analysed for δ^{56}Fe (relative to IRMM-014) with a MC-ICPMS at the Vrije Universiteit (VU) Amsterdam. Values ranged from -0.46‰ to 0.42‰ and showed a trend with negative values at the bottom of the core and more positive values at its top. This trend is interpreted to reflect variations in sedimentation and geochemical cycling in the Mapepe basin induced by changes in basin topography. Negative δ^{56}Fe at the bottom of the core represent incorporation of isotopically light iron in diagenetic minerals, including pyrite, with only minor mixing with sediment input. In contrast, more positive values towards the top of the core suggest a stronger influence of detrital iron derived from weathering of mainly igneous rocks. This is mixed with iron that is withdrawn from the water column by an increasingly active anoxygenic photosynthesis in shallow conditions. A negative excursion of δ^{56}Fe in a unit dominated by volcanoclastic debris coincided with a negative excursion in δ^{34}S and an increase in inorganic carbon. This indicates active sulphur cycling and sulphide production by bacterial sulphur reduction and related Fe withdrawal and pyrite formation.

1. Introduction

Despite intensive research driven by the interest in economically important ores, the emergence of life and the evolution of today's environments, the early earth was perceived as 'hell-like' (Arndt and Nisbet 2012) for most of the 20th century. Its surface was assumed to be hot and inhabitable. During the past two decades, however, the discovery of detrital zircons of Hadean age, most notably from Jack Hills, Australia (Wilde et al. 2001; Valley et al. 2014), changed this view drastically. Other findings like the mass-independent fractionation of sulphur isotopes in rocks older than ca. 2.4 Ga (Farquhar and Wing 2003) helped to reshape our ideas of early earth's environments and geochemical cycling. While we now believe to understand secular changes at the earth's surface, many details stay uncertain. The Barberton continental drilling project is an effort to unravel those details and to give insight into Archean basin dynamics and geochemical cycling with high-resolution basinwide studies of the 3.2 Gya old Fig-Tree group in the Barberton Greenstone belt, South Africa. This study is a part of the Barberton drilling project and focuses on bulk rock iron isotopes in 42 selected reference samples, mainly carbonate-bearing clastic sediments. It aims to investigate sources and sinks of iron as well as early iron cycling in the Mapepe basin and to complement existing iron isotope data. In addition, this study might help resolve the mass-balance issues of isotopically variably Precambrian rocks,

as reported by previous studies (see Johnson et al. 2008b for a review). The goal of this work is to produce a model describing the development of iron deposition in the Mapepe basin.

1.1 The Archean environment

The discoveries of old detrital zircons provided evidence for at least some granitic crust on the early earth. Nowadays, the scientific community agrees that the early earth cooled rapidly after its formation. A continental crust might have developed quickly, but was likely largely submerged under water (Flament et al. 2008). Its growth speed and extent are still debated, and two models are in discussion: a continuous growth model (Albarède 1998) and a rapid crustal growth model (Armstrong 1981). According to the latter, the continental crust reached its current size by ~3.8 Ga. The continuous growth model, on the other hand, predicts only small amounts of continental crust in the early Archean. Independent from the inferred size of crust and continents, surface temperatures were most likely moderate during the Hadean and the early Archean due to a balance between a faint sun and an atmosphere filled with greenhouse gases like CO_2 or methane (Figure 1) (Kasting 1993). In the oceans, hydrothermal systems may have provided suitable habitats for life as early as 3.8 Ga as evidenced in the Isua greenstone belt, Greenland (Rosing 1999; Grassineau et al. 2006). Microbial life was abundant by the mid-Archean and probably widely used anoxygenic photosynthesis to obtain energy (Tice and Lowe 2004). Overall evidence from mass-independent and mass-dependent fractionation of sulphur isotopes suggests anoxic conditions in the early and mid-Archean (Farquhar and Wing 2003; Farquhar et al. 2007; Van Kranendonk et al. 2003), followed by a transformation of atmosphere and oceans in the late Archean (Buick 2008; Canfield 2005). At this time, oxygenic photosynthesis had evolved and promoted the rise of free oxygen concentrations in the earth's atmosphere at ca. 2.4 Ga (Bekker et al. 2004). Ocean geochemistry likely followed the evolution of the atmosphere, and reducing deep oceanic environments became oxidized. Their chemical composition would have been controlled by hydrothermal vents if the majority of the continental crust was indeed submerged, and thereby sediment input into the oceans was small. Hydrothermal sources also provided large amounts of highly soluble ferrous iron. In contrast to modern, oxidized and sulphate-rich oceans, Archean oceans were dominated by iron and carried only low amounts of sulphur.

These ideas about the evolution of the early earth are accepted by most of the scientific community, although there is still debate (e.g. Ohmoto et al. 2006). Many of them originate from research on iron formations, iron rich deposits that were abundant in the Archean (see Bekker et al. 2010 for a review). Their mixture of ferric oxide minerals has evoked interest in the geochemical cycling of iron and, in particular, the oxidation process that removes ferrous iron from the water column. As many experimental studies report iron isotope fractionation during redox cycling, phase changes including mineral precipitation and dissolution, and microbial processes, iron isotopes in Archean iron formations and other rocks can provide important constraints on their formation mechanisms and environmental conditions (Bekker et al. 2010).

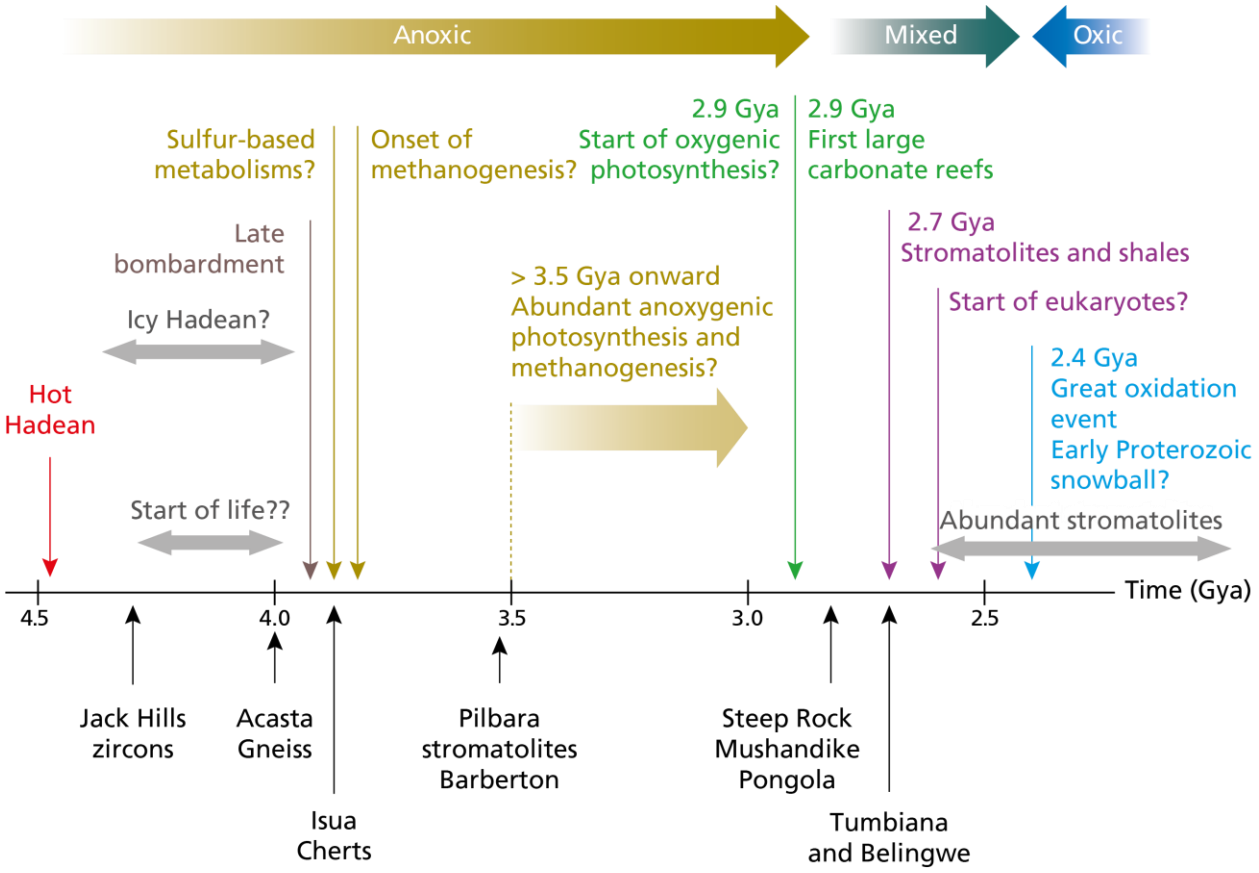

Figure 1: Development of atmospheric composition in time. From Arndt and Nisbet (2012)

1.2 Iron isotopes

The introduction of novel analytical techniques at the turn of the century, especially the advent of multi-collector inductively-coupled mass spectrometers (MC-ICPMS), offered new perspectives for earth scientists. At that point, the potential of techniques involving traditional stable isotopes such as oxygen, nitrogen or carbon had already been thoroughly explored. Analysis of non-traditional isotopes, that is, isotopes of heavy elements with small mass differences, extended the range of applications for isotopic research. Among these non-traditional isotopes, iron is one of the best researched elements so far. Initially, researchers attributed iron isotope fractionation to biogenic cycling of iron (Beard et al. 1999) and therefore generated much interest; the idea to easily trace life in past or extra-terrestrial environments was intriguing and a strong motivation for following studies. Soon, however, investigations showed iron fractionation under abiotic conditions (Anbar et al. 2000) and revealed a number of environments that allow fractionation (e.g. Bullen et al. 2001; Anbar 2004). Nowadays, iron isotope research covers a variety of topics, including those related to earth sciences like Fe pathways in modern oceans, ancient environments or the development of the solar system, or those with a link to life sciences, e.g. the study of human blood (Johnson et al. 2008b). In all of these fields, distinct isotopic signatures have been discovered. On the other hand, the majority of iron in the earth's crust and many of its alteration products have a similar isotopic composition (Beard and Johnson 2004) with ^{56}Fe the most abundant (~91.76%), followed by ^{54}Fe (~5.84%), ^{57}Fe (~2.12%) and ^{58}Fe

(~0.28%.). This unfractionated bulk earth is thus used as a reference for comparison of environments with deviating isotopic composition (Beard et al. 2003). Nowadays, iron isotope studies commonly report those comparisons as δ^{56}Fe values relative to the international iron standard IRMM-014:

$$\partial^{56}Fe = \left(\frac{{}^{56}Fe / {}^{54}Fe_{sample}}{{}^{56}Fe / {}^{54}Fe_{IRMM-014}} - 1 \right) * 10^3$$

Iron in the standard IRMM-014 is slightly lighter (-0.09‰, Beard and Johnson 2004) than in average igneous rocks. All results reported and discussed in this study will follow this notation. So far, observed δ^{56}Fe values range from -3.5‰ to 2.0‰ (see Figure 2 for examples).

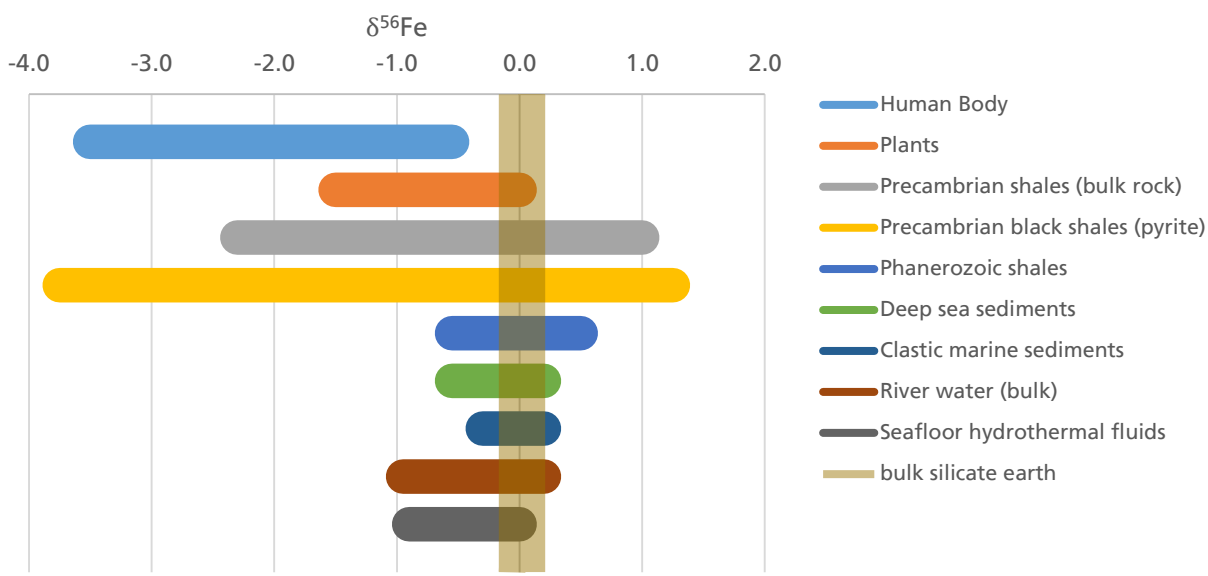

Figure 2: Range of iron isotope fractionation in some environments, modified from Dauphas and Rouxel (2006)

This small range of isotopic variations is related to the mass-dependency of isotopic fractionation. While the electronic structure of an element determines its chemical properties, the mass of the nucleus influences rotational, vibrational and translational movements and hence zero point energies (ZPE) (Bigeleisen 1965). The ZPE of a diatomic molecule AB is $ZPE = 1/2h\nu$ with the vibrational frequency of the bond ν and Planck's constant h (Anbar and Rouxel 2007; Schauble 2004). If the movement of the bond is approximated as a harmonic oscillator, the vibrational frequency can be expressed as $\nu = 1/2\pi\sqrt{k/\mu}$ with the force constant k and the reduced mass of the bond $\mu = m_A m_B / (m_A + m_B)$. Since ZPE govern bond strengths, and the ZPE of a diatomic molecule AB is a function of the masses A and B, bond strengths are also mass dependent (Figure 3). In general, energy differences between the molecule and dissociated atoms increase when the ZPE decreases. Consequently, bonds involving heavy isotopes are stronger due to lower ZPE.

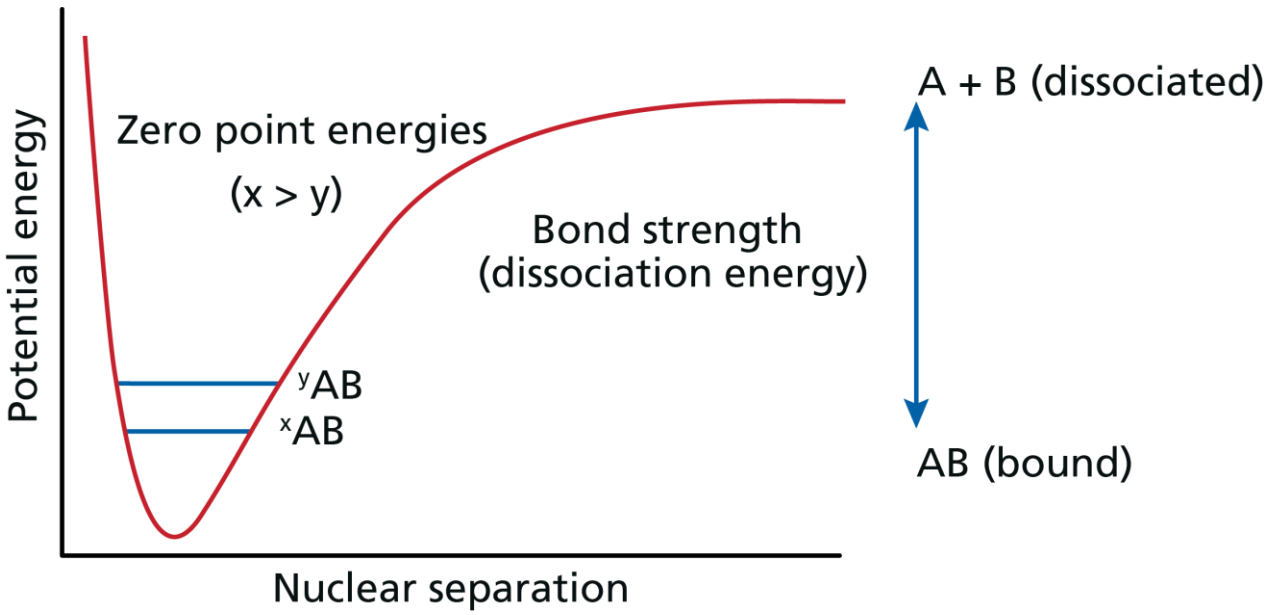

Figure 3: Relationship between Zero point energies and dissociation energy for two molecules AB with different isotopes of A. Modified after Bigeleisen (1965)

On the contrary, bonds involving light isotopes are broken easier. The light isotope is therefore enriched in the products of a unidirectional or incomplete reaction, and this process is called kinetic isotope fractionation. If reactant and product are separated during the reaction, isotopic ratios will ultimately be determined by the extent of the reaction (Rayleigh fractionation). "Equilibrium isotope fractionation" denotes any fractionation from processes involving both forward and backward reaction. Here, differences in the distribution of isotopes also arise from differences in ZPE and stabilities of phases.

To date, experimental and analytical studies have described a wide range of processes that fractionate iron isotopes, covering high and low temperature environments. As high temperature environments and associated fractionation processes, that is, diffusion, evaporation, condensation and phase partitioning, (see Dauphas and Rouxel 2006 for a review) are not the subject of this study, only low temperature mass fractionation of iron will be further discussed. Among the principal factors that govern iron mass fractionation are redox processes (Anbar and Rouxel 2007): isotopic fractionation has been reported for dissimilatory iron(III) reduction (DIR) (Beard et al. 2003; Icopini et al. 2004), anaerobic photosynthetic iron(II) oxidation (Croal et al. 2004), abiotic iron(II) oxidation and subsequent precipitation of ferric oxyhydroxides (Bullen et al. 2001) or sorption of aqueous iron(II) onto ferric oxyhydroxides (Icopini et al. 2004). Microbially mediated reduction or oxidation of iron is of particular interest; these processes are directly linked to carbon cycling, and both cycles interact with the sulphur cycle. During DIR, microbes use iron as electron acceptor for the oxidation of organic carbon. As lighter bonds are broken easier, DIR releases light ferrous iron along with inorganic carbon[1]. This process is reversed during anoxygenic photosynthetic Fe^{2+} oxidation, when isotopically light organic carbon is produced. Many have argued that the latter reaction

[1] DIR can be expressed as: $4Fe(OH)_3 + CH_2O + 8H^+ \longrightarrow 4Fe^{2+}_{aq} + CO_2 + 11H_2O$ (Johnson et al. 2008b)

was used by the earliest organisms given the abundance of iron in the Archean oceans (Raiswell and Canfield 2012). Both processes fuel each other because DIR requires reactive ferric iron and organic matter as produced by anoxygenic photosynthetic Fe^{2+} oxidation, whereas anoxygenic photosynthetic iron oxidation uses dissolved ferrous iron and CO_2. Observed fractionation ranges from very negative values of up to -3.5‰ for the products of DIR, to positive values around 1‰ for the products of coupled oxidation and precipitation of iron oxides (Johnson et al. 2008b).

Sulphur and carbon are linked in a similar way with bacterial sulphate reduction providing new inorganic carbon and isotopically light sulphide and bacterial sulphide oxidation delivering new sulphate. Iron and sulphur cycle interact during the sequestration of iron-sulphur minerals; sulphide is barely soluble and readily reacts with ferrous iron to form iron-monosulphides or pyrite. Iron and sulphur isotopes in these compounds may reflect a range of processes, including DIR and BSR, as well as equilibrium or kinetic fractionation during mineral formation (Johnson et al. 2008b). Nonredox processes may produce a weak but significant fractionation, too, and include inorganic mineral precipitation of oxides (Beard and Johnson 2004), carbonates (Wiesli et al. 2004) or sulphides and equilibrium isotopic exchange with these minerals and their precursors (Butler et al. 2005).

Next to the experimental investigations of iron isotope fractionation, a growing number of studies explored iron isotopic variations in Archean rocks, in particular iron formations. Observed long-term variations are similar to Precambrian bulk shales or sedimentary pyrite and indicate limited fractionation with near-zero and slightly positive $\delta^{56}Fe$ values in the early Archean (Johnson et al. 2008b; Bekker et al. 2010) and strong fractionation between 3.1 and 2.5 Gya with a wide range of values, including very negative ones (-3.5‰ to 1.5‰). After 2.4 Gya, the extent of iron isotope variation decreases again and most reported values cluster around the bulk crustal average. This secular isotopic record is interpreted to reflect partial oxidation of dissolved ferrous iron by anaerobic photosynthesis in the early Archean (Planavsky et al. 2012), followed by increased iron cycling in the middle to late Archean. Due to the slow rise of oxygenic photosynthesis and hence an increasing supply of ferric iron and organic carbon, dissimilatory iron reduction bloomed and peaked between ~2.7 and 2.5 Gya. Notable concentrations of free oxygen were probably first produced only locally in certain settings, e.g. basins, before influencing the oceans at the end of this period. The strong increase in atmospheric oxygen contents at ~2.4 Gya eventually removed most iron in the oceans when deep waters became oxidized. As the cycled iron inventory becomes much smaller, the range of recorded iron fractionation decreases (Johnson et al. 2008b).

Iron in many iron formations is derived from hydrothermal vents, bulk seawater or late-stage fluids and its isotopes can reflect either seawater composition, diagenesis, or fluid alteration. Predominantly clastic sediments like shales, in contrast, are also strongly influenced by iron with terrestrial origin. Constraints on the isotopic signature of various iron sources should thus be established for studies like this one. Hydrothermal vents are the principal sources for iron in early deep oceans. Modern hydrothermal fluids have negative $\delta^{56}Fe$ values that are positively correlated to their iron concentrations. Johnson et al. 2008a interpreted this relationship as the interplay between crustal dissolution and formation of exhalites which have more negative $\delta^{56}Fe$ values. They argue that higher heat flows and iron fluxes in the Archean likely produced a higher degree of crustal dissolution and therefore an isotopic signature close to the crustal average. Still, precipitation of diagenetic minerals could have altered those fluids (Yamaguchi et al. 2005).

Terrestrial iron sources include volcanoclastic input or weathering of igneous or sedimentary rocks. If the atmosphere was indeed more acidic[2] and weathering was more intense than today, bulk rock[3] weathering produced large quantities of mobile iron that could be cycled and potentially fractionated. However, the Archean atmosphere was anoxic and redox changes were absent. Therefore, significant fractionation is unlikely. In case of volcanoclastic fragments that were delivered to the oceans either directly by an eruption or indirectly by rivers, the isotopic signature should thus be close to the igneous rock average. Other source rocks likely retained their original isotopic composition.

1.3 The Barberton greenstone belt and the Mapepe basin

This study deals with iron isotopes in rocks of the Barberton greenstone belt, a NE-SW striking succession of metamorphosed Archean volcanic and sedimentary rocks that is surrounded by a variety of granitoids (Figure 4). It is located on the Kaapvaal craton in north-eastern South Africa at the border of Swaziland. The Barberton greenstone belt has been an important example for research on Archean greenstone terrains and a number of studies have investigated its stratigraphy, geochemistry and tectonic development, for instance Lowe and Nocita 1999; Lowe and Byerly 1999 or Hofmann 2005 whose findings are summarized in this section. It consists of three tightly folded stratigraphic units ranging in age from ca. 3550 to 3220 Ma (Hofmann 2005): the Onverwacht, Fig-Tree and Moodies group. The belt is divided by a major fault zone called Inyoka fault. Although severely deformed, most rocks are only moderately altered by metasomatism and metamorphism compared to other rocks of similar age.

[2] Due to higher CO_2 levels

[3] Mineral weathering is preferential and releases light isotopes first. This fractionation is irrelevant if weathering is complete.

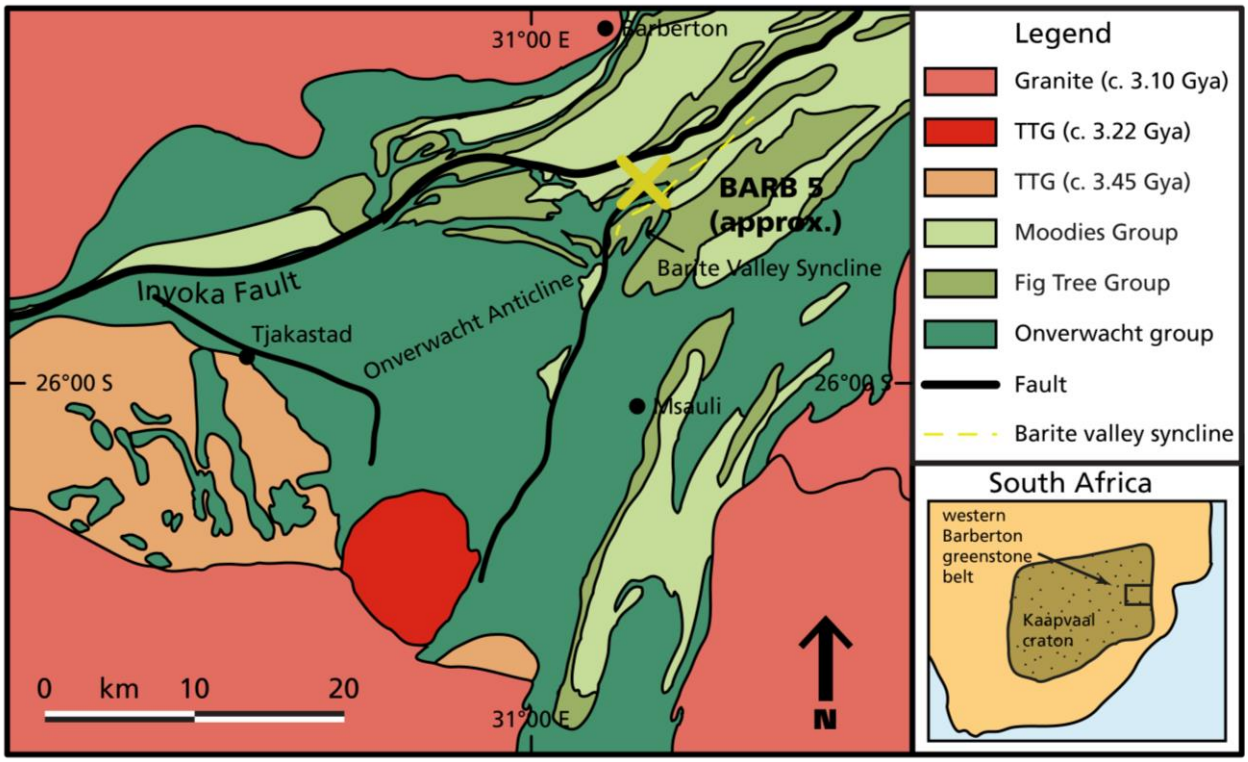

Figure 4: Simplified geological map of the Barberton greenstone belt, South Africa. Modified after Hofmann, Harris (2008)

The Onverwacht group is the oldest of the three units of the Barberton with ages between 3550 and 3300 Ma. It mainly consists of thick sequences of (ultra-)mafic igneous rocks, ranging from komatiites to basalts, with minor felsic volcanic and thin interbedded sedimentary rocks and one ferruginous chert unit ('Buck Reef Chert'). Most of the Onverwacht group is weakly metamorphosed up to greenschist-facies conditions, except for parts in contact with surrounding granitoids (up to amphibolite-facies). Some of the komatiitic sequences were affected by strong metasomatism and silicification (Hofmann and Harris 2008). On the other hand, the youngest unit named Moodies group only consists of quartzose and feldspathic sedimentary rocks that were deposited in shallow to fluvial settings. The Fig-Tree group contains ca. 3259 to 3225 Ma old (Krüner et al. 1991) clastic and chemical sediments that were formed between Onverwacht and Moodies times and will be discussed later in more detail. Both Fig-Tree and Moodies group occur in two distinct sequences north and south of the Inyoka fault, which is interpreted as a tectono-stratigraphic boundary that divides different depositional environments within one large basin with similar but distinguishable sources (Lowe and Byerly 1999).

Three iron rich units have been described within the Barberton greenstone belt: the Buck Reef Chert in the Onverwacht group, a jaspilitic iron formation in the lower part of the Fig-Tree group called Manzimnyama jaspilite, and a banded iron formation (BIF) in the Moodies group. Both Buck Reef Chert and Manzimnyama jaspilite are comprised of abundant siderite and jaspilite bands with additional hematite layers in the Manzimnyama jaspilite (Lowe and Byerly 2007). In the Moodies group BIF, iron is mainly present in hematite, magnetite and ankerite (Bontognali et al. 2013).

The rocks obtained from the Barb5 drill core are located south of the Barite valley and belong to the Mapepe formation. This formation is part of the southern Fig-Tree group and overlies the Manzimnyama jaspilite. Former studies described this unit as a variety of "chert clast conglomerate, micaceous and carbonate-cemented sandstone, green and grey chert, and detrital barite sandstone" (Hofmann 2005) in its lower part. The upper part consists of shales and siltstones with sedimentary flow features and minor sandstones and conglomerates. According to Lowe and Nocita (1999), the Mapepe sediments are derived from weathering of the Onverwacht group and contemporaneous volcanic activity, and reflect three depositional environments: a) a quiet basin with subaqueous sedimentation, b) a fan-delta and c) shallow-water conditions. Primary and diagenetic minerals are commonly preserved in the Mapepe formation and other sedimentary units of the Barberton greenstone belt (Lowe and Byerly 2007), but geochemical analysis (Hofmann 2005) of various rocks from the Fig-Tree group indicates depletion of many mobile elements due to hydrothermal alteration, possibly during several events.

Current Sedimentological analysis of the 800m deep Barb5 drill core (Figure 5, Drabon et al., pers. comm.) corroborates the broad concept of Lowe and Nocita (1999). A sequence of pyrite-rich carbonaceous shales and mudstones at the bottom of the core is overlain by clastic sediments with increasing grain size (see figure 5). At 260m core depth, corresponding to ~130m of stratigraphic depth, the fraction of volcanoclastic components, lithics and green ash in the sediment increases drastically. The volcanoclastic sand disappears in the upper part of the core, where small shale units are disrupted by fining-upward sand sequences. Drabon et al (pers. comm.) interpret this as shoaling basin that is interrupted by volcanoclastic sand deposition. Towards the end of Mapepe sedimentation, the sedimentary environment was affected by low density turbidity currents.

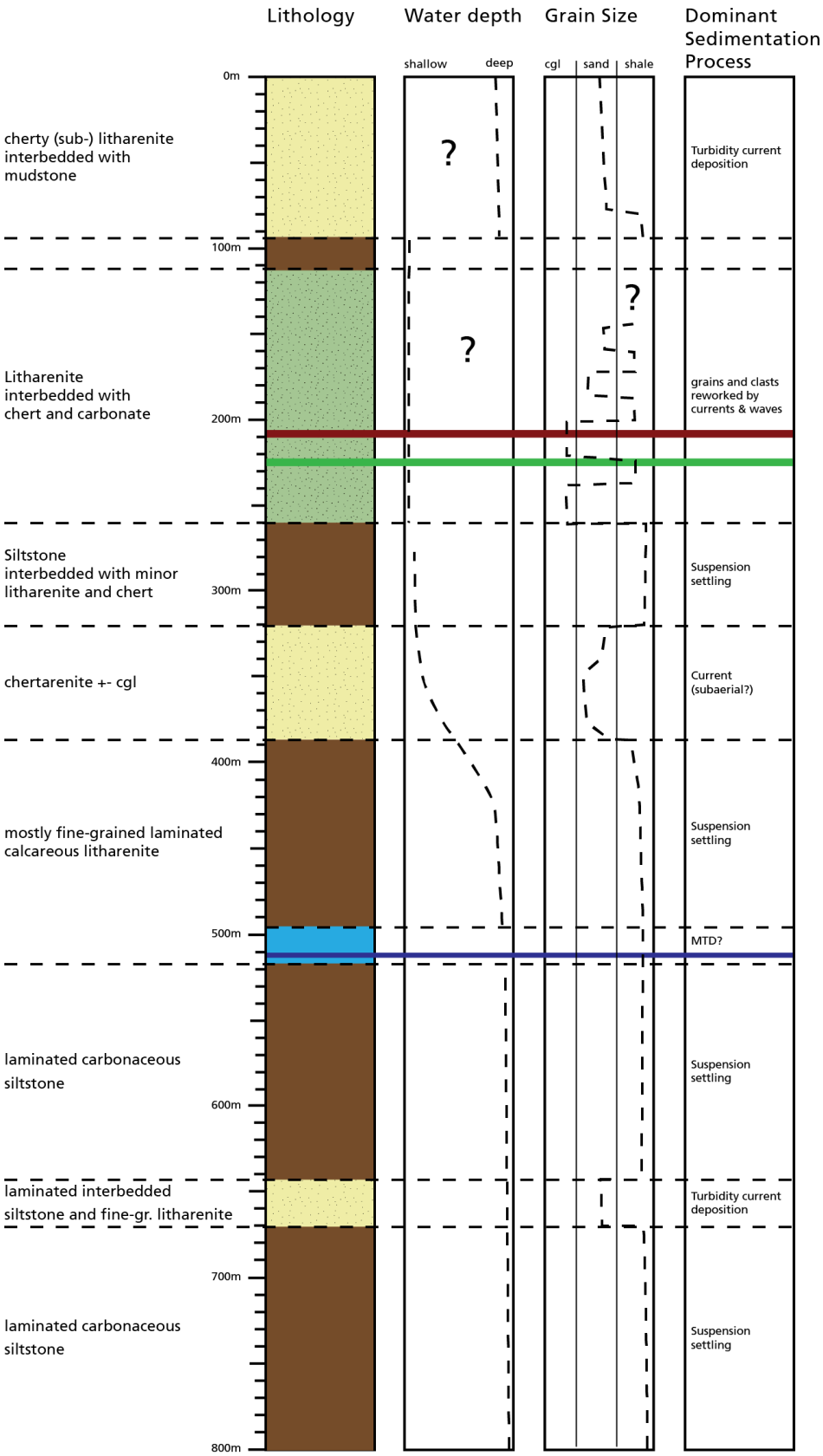

Figure 5: simplified core log of the Barb 5 drill core depicting lithologies and inferred depositional environment. From Drabon et al. (pers. comm.).

2. Methods

In this study, 42 sample powders obtained from the Barberton 5 drill core were selected and processed for bulk iron isotope analysis. All Teflon labware was cleaned in hot pro analysis quality HNO_3 and HCl solutions, with an additional step of cleaning with double distilled (DD) 7M HCl, closed at 120 °C on a hotplate. Reactants used in this study were DD (HCl) or double Teflon distilled (DT) (HNO_3, HF).

Iron was chemically separated from the rock matrix using the method of (Dauphas et al. 2004; Dauphas et al. 2009b) with the following modifications. First, preliminary XRF Fe concentration data were used to estimate the sample amount necessary for processing ~300 µg Fe in total, which typically ranged from 2-6 mg of powder and was kept below 20 mg. Subsequently, the sample powders were digested with hydroflouric acid, nitric acid and hydrogen perchloride and oxidized, as outlined in the protocol in Table 1. A fraction of the sample was then purified during a chromatographic column procedure with an anion exchange resin (Biorad AG1-X8 200-400 mesh). This iron separation procedure is repeated twice to ensure complete elimination of matrix elements. Afterwards, both the iron fraction and the remainder of the digested sample were dried down and dissolved in 1% DT HNO_3.

In order to identify potential loss and fractionation of iron isotopes during the purification procedure (Anbar et al. 2000), Fe concentrations of the solutions were compared using a Varian 720-ES ICP-OES which yields instrumental precisions better than 2%. Our results indicate an effective removal of potentially interfering matrix elements and only minor loss of iron. Five samples did not match the desired yield of 100 +/-3%, but iron isotope analysis suggests negligible fractionation as discussed in Appendix 5.3.

All isotope measurements were performed on a ThermoFinnigan Neptune MC-ICPMS at the VU University, Amsterdam, equipped with a Cetac Aridus I desolvating nebulizer. Analysis followed the technique suggested by Weyer and Schwieters (2003) who used high mass resolving powers of 8000-9000 to resolve interferences of isobaric polyatomic ions (e.g. $^{40}Ar^{16}O^+$ on $^{56}Fe^+$) and a sample-standard bracketing technique to correct for instrumental mass bias. Results are reported in the delta notation relative to IRMM-014 (Dauphas et al. 2004). An instrumental precision of ~0.16 ‰ (2SD, n=29) was achieved with repeated measurements of an internal iron standard solution. International geological standards that were also processed yielded average $\delta^{56}Fe$ values of 0.10‰ for BHVO-2, 0.09‰ for MAG-1 and 0.045‰ for SGR-1 that compare well with published results within the range of error (Craddock and Dauphas 2011; Wang et al. 2012; Beard et al. 2003; Dideriksen et al. 2006; see table 2).

Table 1: Chemical procedure for preparation of samples for Fe isotope measurements, modified from (Dauphas et al. 2004; Dauphas et al. 2009b)

- **Digestion**: Addition of ~25 drops conc. HF, ~12 drops conc. HNO_3 and one drop conc. $HClO_4$
- Heating in closed beakers at 140°C for at least 24h
- **First Oxidation step**: Cooling down, evaporation for 2-3h at 120°C, cooling down and addition of 150 µl H_2O_2 (31%)
- Heating with closed lit at 120°C for 1h and evaporation at 150°C
- **Second Oxidation step**: Addition of two drops conc. HNO_3, one drop $HClO_4$ and 50 µl H_2O_2. Drying down at 150°C; Redissolution in 2 ml 6 M HCl + 0.001% H_2O_2
- **Column preparation**: Disposable Bio-Rad Poly-Prep polyethylene columns are filled with 1 ml of AG1-X8 200-400 mesh Cl-form anion exchange resin
- **Precleaning sequence for resin**: 10 ml H_2O, 5 ml 1M HNO_3, 10 ml H_2O, 10 ml 0.4M HCl, 5 ml H_2O, 2 ml 6M HCl
- The resin is preconditioned with 3x 1 ml 6 M HCl + 0.001% H_2O_2

- Loading of 1-1.3 ml sample onto the column. The remainder is dried down at 120°C
- **Elution of matrix**: **:** 1 ml 6M HCl + H_2O_2, repeat one time, 2 ml 6M HCl + H_2O_2, 4 ml 6M HCl + H_2O_2
- Change beakers to collect iron
- **Elution of Fe**: 3x 3 ml 0.4M HCl
- Evaporation at 120°C, reoxidation with two drops H_2O_2; the sample is left with closed lit for one hour and subsequently dried down at 120°C. Redissolution in 0.5 ml 6 M HCl + 0.001% H_2O_2
- The resin is suitable for a second re-use when precleaned with 10 ml 6-7 M HCl, 10 ml H_2O. If visibly dirty, the resin should be replaced. If needed, columns were stored in 0.165 M HCl
- The column procedure is repeated a second time.
- After drying down the sample, both the Fe fraction and the remainder of the digested sample were dissolved in 2 ml 1% HNO_3. The samples are now ready for analysis with ICP-OES and MC-ICPMS.

Table 2: Selected published values for the geological standards BHVO-2, MAG-1 and SGR-1 that were processed in this study. Our measurements yielded δ^{56}Fe values of 0.10‰ for BHVO-2, 0.09‰ for MAG-1 and 0.045‰ for SGR-1

Standard	Value (δ^{56}Fe)	Publication
BHVO-2	0.114 +/- 0.011 (2SD, n=12)	Craddock, Dauphas 2011
	0.102 +/- 0.012 (2SD, n=7)	Wang et al. 2012
	-0.03 (average, n=2, SE for individual measurements: 0.07)	Dideriksen et al. 2006
MAG-1	-0.04 +/- 0.14 (2SD, n=2)	Beard et al. 2003
	0.13 +/- 0.06 (2SE)	Dideriksen et al. 2006
SGR-1	0.036 +/- 0.015 (2SD, n=5)	Craddock, Dauphas 2011
	-0.36 +/- 0.3 (2SD, n=2)	Beard et al. 2003
	0.15 +/- ?	Dideriksen et al. 2006

3. Results and Discussion

Measured δ^{56}Fe values for the rocks of the Barb 5 drill core range from -0.46‰ to 0.42‰ (Figure 6) with a weighted average of ~0‰. A weak trend from slightly negative values at the bottom of the core to slightly positive values at the top was observed. At a depth of ~250m to 200m, a negative excursion interrupts this trend. When compared to the stratigraphic profile and the inferred development of the depositional environment, the section of the core with lighter iron was generally found in areas with deep basin sedimentation, whereas heavier iron coincided with shallower environments, including alluvial fans. The negative excursion coincided with the first occurrence of the volcanoclastic unit in the core. Montinaro (pers. comm.) reports δ^{34}S isotope and organic (TOC) and inorganic carbon (TIC) data for the Barb 5 core that also show a negative excursion for δ^{34}S in addition to a strong increase in TIC at the base of the volcanoclastic unit. Furthermore, measured organic carbon concentrations are highest in the lowest part of the core where iron was particularly light at values up to 2%. Unlike the negative excursion, the weak continuous trend in iron isotopic composition cannot be related to sulphur isotopes.

Hereafter, the part of the drill core representing predominantly volcanoclastic deposits (ca. 250-110m depth) will be referred to as “volcanoclastic unit”, while “bottom” or “lower” unit denotes the part of the core below the volcanoclastics.

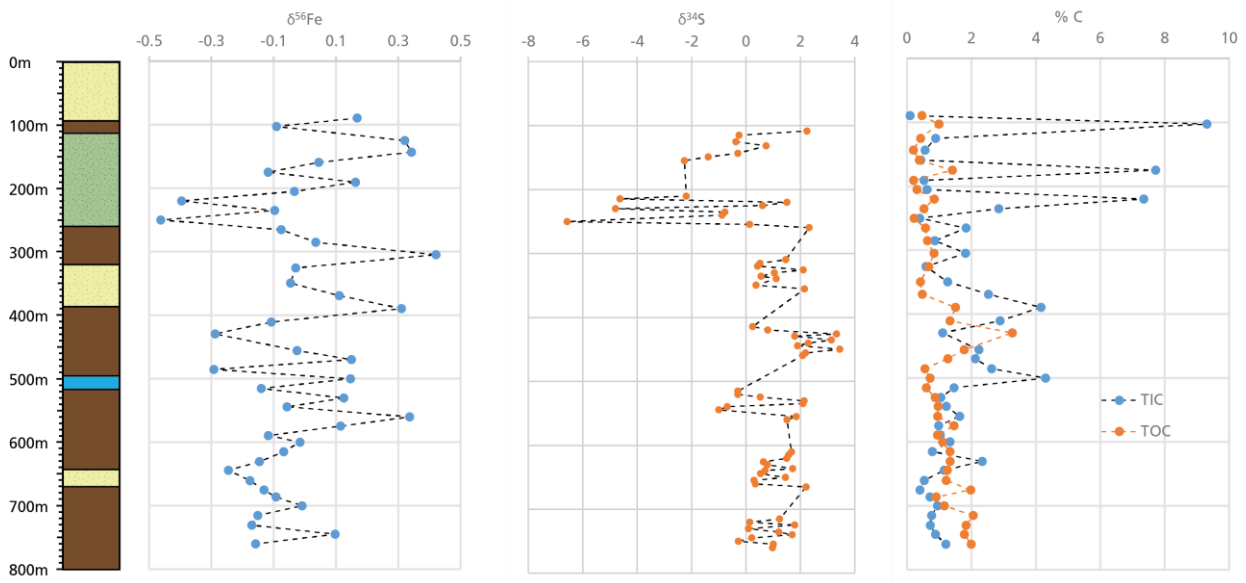

Figure 6: Variation of iron and sulphur isotopes and total inorganic and organic carbon concentrations in 42 selected reference samples

3.1 Geochemistry of Barb 5 sediments

Geochemical analysis of the Barb 5 drill core were performed by Galic et al. (in prep.). Total concentrations of some transition metals like Ti, V, Cr, Ni or Cu showed an upwards decreasing trend in the core's bottom unit, but varied in the volcanoclastic and upper unit. Grain-size (Al) normalized concentrations of transition metals increased upwards in the lowest part of the core, and showed a rapidly decreasing top with some scatter. Normalized iron concentrations were flat and showed only minor variation in shale units, whereas coarser parts of the core coincided with greater variability. Positive spikes in Al-normalized Fe concentrations were observed at 735m and 500m core depth and in the volcanoclastic unit. Grain-size normalized concentrations of more mobile elements like K or Rb showed a distinct pattern (Figure 7) that cannot be related to the variation of immobile elements. Na mirrored this trend as it was enriched in sections where K or Rb was depleted. Areas with the strongest enrichment of Na and strongest depletion of K or Rb within the lower shale-dominated unit roughly coincided with sections with relatively high amounts of coarse material. Rare earth element (REE) patterns did not show any trends related to core depth, they were rather flat when normalized to post-Archean Australian shale (Taylor and McLennan 1985), although all had a positive Eu anomaly. Total REE were low in the shales in the lower part of the core and increased in the volcanoclastic unit. Y/Ho ratios clustered around a value of 32. Iron speciation data (Montinaro, pers. comm.) for shales was used to calculate highly reactive iron (FeHR) (Poulton and Canfield 2005) and degree of pyritisation (DOP) (Raiswell and Canfield 2012). Values ranged from ~0.4 to 0.8 for the highly reactive iron/total iron (FeT) ratio and up to ~0.3 for DOP (figure 8). In general, samples in the lower section of the core exhibited lower FeHR/FeT ratios and higher DOP.

The sediments are interpreted to reflect a mixing of mafic and felsic components (see also figure 7), with an enrichment of felsic components at the top of the core. Variation of mobile elements suggests post-depositional K-metasomatism similar to a process described by Hofmann and Harris (2008) and Rouchon

et al. (2009), which has a grain-size controlled effect on the sediment geochemistry. Positive Eu anomalies (Eu/Eu* shale normalized) (Planavsky et al. 2010) further corroborate the notion that the sediments are affected by hydrothermal activity (Michard and Albarede 1986; Bau 1991). Patterns in Eu anomalies similar to the K-metasomatism are absent and estimation of the timing of REE's hydrothermal overprint is difficult. Hydrothermal fluids can cause changes in REE signatures in either the sediments (syn-depositional or late stage alteration), volcanic source rocks that had a low total REE, or both. Observed Y/Ho ratios are slightly super-condritic (chondrites: 26-28, Hofmann 2005) and can be compared to the values of cherts from the Fig-Tree group reported by Hofmann (2005), who interpreted this as a partial preservation of a seawater signature. Lastly, iron speciation data indicate an anoxic, ferruginous environment (figure 8) for the formation of Fe phases.

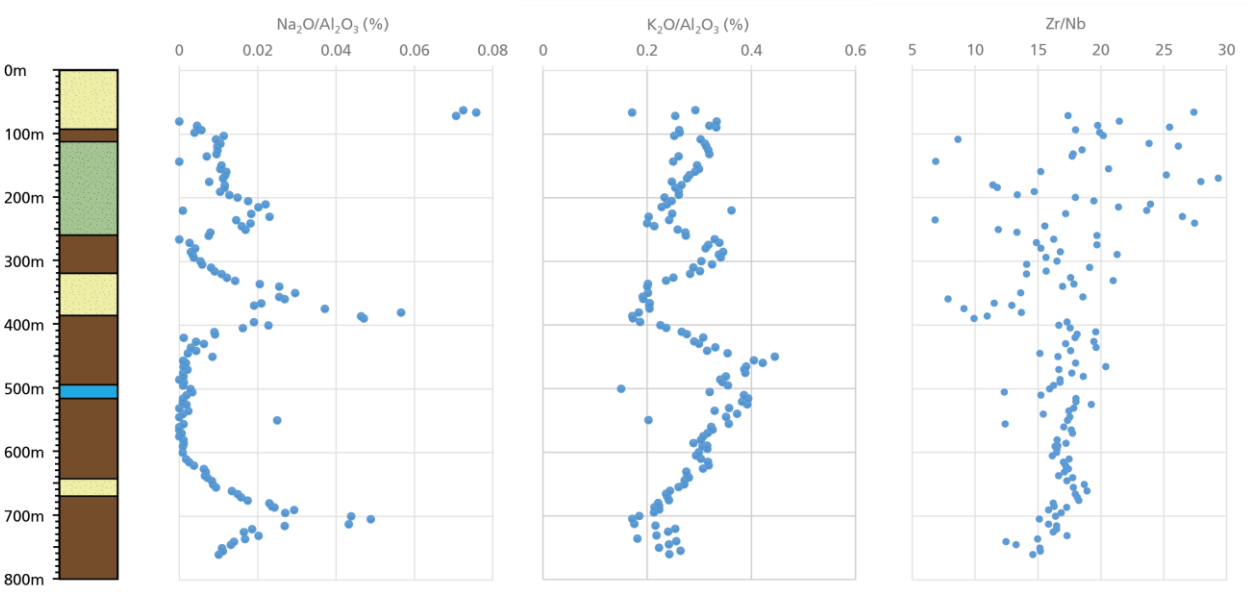

Figure 7: Observed variations in aluminium normalized Na and K concentrations that were interpreted as alteration product, and the Zr/Nb ratio throughout the Barb 5 drill core which reflects more mafic components at the bottom and more felsic at the top

3.2 Origin of iron

In today's world, iron has a critical role for most organisms. It is an important micronutrient that rivers, icebergs, aeolian dust or hydrothermal vents transport to the oceans. Here, availability is limited since any reduced iron is rapidly oxidized and precipitated as iron oxyhydroxide. Nonetheless, complete removal of iron is slow, and current residence times are in the order of 10^4 years (Johnson et al. 2008b).

Residence times of iron in the Archean oceans were likely even longer than present-day because of iron's redox state and the higher concentrations of dissolved iron. Despite these differences between the modern and historic oceans, iron was still vital for organisms. Instead of only being a micronutrient, iron is assumed to be the main source of energy for the majority of the Archean microbial community; anoxygenic photosynthesis and iron reduction were likely much more important in ferruginous oceans and are assumed to make up for 1/24-1/8 of today's primary production (Raiswell and Canfield 2012). Consequently, iron in

sediments might be strongly influenced by microbial activity, and microbial iron oxidation may exert a major control on its deposition as discussed in case of many iron formations (Bekker et al. 2010). If, however, iron cycling occurs only locally and the size of the reservoir is restricted like in the Mapepe Basin, residence times will potentially be much shorter. The detrital sources of iron in the Barb 5 core could have dominated the depositional processes, therefore the potential of detrital control of iron sequestration in the basin is discussed first.

Indeed, the covariation of iron isotopes, transition metals, and the inferred topography of the Mapepe basin based on the Barb 5 core suggests such a control on iron sequestration. The correlation between iron concentrations or δ^{56}Fe and petrogenetic indicators, such as Th/Sc, Zr/Nb or La/Yb ratios, is very weak. A regression line for δ^{56}Fe (excluding the volcanoclastic succession) was also matched with these ratios, but similarly provided a poor fit; this indicates that bad correlations are not caused by variation in δ^{56}Fe due to instrumental error. Missing relationships between total iron concentrations and concentrations of transition metals are particularly notable as they should generally behave similarly. This suggests an absence of a direct link between the composition of igneous source rocks and iron deposition, thus reflecting either small amounts of iron in the source rocks or high residence times coupled with another iron deposition mechanism besides the settling of iron-bearing clasts. A possible explanation is the metasomatic alteration and leaching of volcanic rocks from the Onverwacht group, as reported by Hofmann and Harris (2008) and Rouchon et al. (2009). These rocks are enriched in K, Rb and Si and depleted in some other elements including Na and Fe. If the source rocks for Mapepe sediments were similarly depleted in iron, detrital material would have had only a minor control on iron in sediments as opposed to iron derived from seawater and hydrothermal activity. Otherwise, if there was no iron depletion, higher residence times are likely to have caused the observed weak correlations. The fine-grained structure of rocks at the bottom of the core does suggest deep basin sedimentation, which could be a reason for the extended residence times. This implies that samples obtained from sandstones or conglomerates were subject to shorter residence times and thereby more directly reflect their sources.

So far, this discussion is based on the assumption that only volcanic rocks of the Onverwacht group and contemporaneous volcanic activity determine the sedimentation in the Mapepe basin. However, the range of iron isotopic composition is too high to be solely derived from igneous rocks because only low amounts of fractionation have been measured during igneous petrogenesis (e.g. Wang et al. 2012; Dauphas et al. 2009a). Not only are these variations much lower than the range observed in the Barb 5 drill core, also, any fractionation in igneous rocks only distributes isotopes among different minerals and bulk rock weathering should result in iron values clustering around a 0.09‰ crustal average. This explanation matches the slightly positive δ^{56}Fe values observed in coarser sediments at the top of the core that could better reflect the isotopic composition of sediment sources. Still, iron at the very top of the core is too heavy to be derived only from sediment input. Besides the Onverwacht group, parts of the lower Fig-Tree group have been proposed as source regions (Hofmann 2005). Increased mixing with iron-rich rock detritus with positive δ^{56}Fe values, for instance the Manzimnyama jaspilite (Planavsky et al. 2012), would explain the observed trend in iron isotopes. Such iron rich detritus was indeed observed in the drill core, but rough estimates of its abundance suggest that iron formations do not primarily control iron concentrations in the coarse sediments.

Metasomatic processes also directly influenced the sediments in the Mapepe basin, as shown by characteristic variation patterns in K, Rb or Na concentrations. Contrary to the observations in rocks of the Onverwacht group, this alteration is not expected to significantly influence iron composition since neither iron concentrations nor $\delta^{56}Fe$ link to these patterns. Trends in concentrations of transition elements with similar chemical behaviour are also not related to variations of mobile alkali metals. This indicates that these elements were not affected by fluid leaching or enrichment. Measured iron isotopic values should thus still reflect the original composition during deposition.

3.3 Sequestration of iron from the seawater

If the iron isotopic composition in the samples was not primarily controlled by a variation in sediment input or late-stage alteration, geochemical cycling and diagenesis must have had a strong influence on the sequestration of iron from seawater. Unfortunately, the range of possible mechanisms is large, and discrimination between them is tedious. Hence, the two models discussed in this section are based on the hypothesis that alterations in basin topography and related environmental conditions, such as the fraction of the basin penetrated by light or seawater temperature, induce changes in geochemical cycling or deposition.

The distribution of iron mineralogies within the core suggests at first glance a mineralogical control on the iron composition. Nowadays, pyrite is found in greater abundance in the shales of the lower section of the Middle Mapepe formation while iron carbonates dominate the upper part. If these are primary minerals, the key to the pattern in $\delta^{56}Fe$ could lie in iron fractionation during mineral formation. Primary carbonates are known to be rare in the Archean, when high levels of dissolved CO_2 caused acidic environments that could hamper carbonate precipitation. Nevertheless, conditions for carbonate precipitation could exist, especially in a shallow basin with elevated temperatures. So far the rocks from the Barb 5 drill core have been regarded as suitable examples for a potential carbonate-bearing site in the Archean, but new geochemical investigations question this idea. Comparisons of *in situ* data of carbonates in cross-cutting veins to matrix carbonates (Galic and Mason, pers. comm.) reveal great similarities and suggest that both were formed during a single event. A sound interpretation has yet to be delineated and further analytical work possibly remains to be completed, but other considerations also confirm that primary carbonate precipitation was unlikely to be in control of iron isotopic composition. Experimental iron-carbonate precipitation does lead to enrichment of light isotopes in the solid phase (Wiesli et al. 2004). This contrasts with the trend observed towards heavier iron isotopes and suggests that iron was not drawn from a big pool, e.g. during precipitation of carbonates from seawater.

More possibilities are open for the interpretation of the isotopic record once the iron carbonates in Barb 5 are regarded as potential secondary replacements of other iron-bearing phases. Fractionation of heavy iron (~1‰) was reported for iron(III) oxyhydroxides, such as ferrihydrite, which are produced by partial oxidation of ferrous iron and subsequent precipitation of a mineral phase (Beard and Johnson 2004). Iron oxidation is a rapid process in modern oxidized oceans. In the past, this oxidation step was much slower due to the absence of significant amounts of free oxygen during most of the Archean and quantitative iron oxidation probably relied on microbial catalysis by anoxygenic photosynthesizers (Bekker et al. 2010). Their

effect on the overall composition of a water body should be related to its depth; in a shallower environment the fraction of the water body penetrated by light - the fraction suitable for anoxygenic photosynthesis - is higher than in a deep basin. In the case of the Mapepe basin, this assumption argues in favour of a heavy iron enrichment in the shallow sedimentary environments. Due to the reactive nature of iron oxyhydroxides, transformation by diagenetic or late-stage CO_2-rich fluids into iron carbonates is then possible while still retaining the original isotopic signature.

Nevertheless, negative $\delta^{56}Fe$ values at the core's bottom indicate that mechanisms and sources other than anoxygenic photosynthetic iron oxidation must have played a role, too. In the shales of this section of the core, pyrite is more abundant. Kinetic fractionation during the formation of pyrite precursors has been noted in experiments and typically shows an enrichment of light isotopes in the solid phase relative to the fluid phase (Butler et al. 2005). Fractionation decreased with aging in these experiments, but minimum values that might represent equilibrium are still negative at ca. -0.3‰ for FeS. Furthermore, seawater at this time could have been enriched in light iron isotopes. Planavsky et al. (2012) have measured positive $\delta^{56}Fe$ for some iron formations, including the underlying Manzimnyama jaspilite, and interpreted this as iron enrichment by anoxygenic photosynthesis, which leaves light isotopes in the water column. At this point, the influence of either effect, diagenesis of pyrite or seawater composition, can only be speculated, but *in situ* measurements of iron isotopes in pyrites could potentially back up this hypothesis. Pyrite should then be isotopically lighter than other minerals or the bulk composition of the core if fractionation during pyrite formation is a relevant process.

3.4 Influence of the volcanoclastic unit

In the upper portion of the Barb 5 drill core, correlation of negative excursions of $\delta^{56}Fe$ and $\delta^{34}S$, a spike in inorganic carbon, and sedimentological analysis that argues in favour of intensified volcanic activity all indicate a change in depositional environment or geochemical cycling. A direct control of volcanic debris on sedimentation should shift the iron isotopic composition towards the crustal igneous average. Since the opposite was observed, it is more likely that other mechanisms control iron deposition. In addition to the variation in the above mentioned parameters, sulphur contents of the sediments also show a positive spike at the onset of the volcanoclastic unit (figure 8). Fractionation of sulphur towards lighter isotopes occurs during bacterial sulphate reduction (BSR). Since fractionation is largest if sulphate is available in excess (Canfield 2001, cited in Johnson et al. 2008b), it can be assumed that the general activity of BSR is proportionate to sulphate availability. The small range of fractionation observed in Archean rocks has thus been interpreted as a product of sulphate-limited BSR. If volcanic activity transported substantial amounts of sulphur to a generally sulphur-poor Mapepe basin, and if larger amounts of dissolved sulphate concentrations were produced, BSR could have had a similar effect and produce observed sulphur fractionation of up to -7‰ (figure 6). As BSR uses sulphate as the terminal electron acceptor to oxidize organic carbon in order to gain energy, another product of BSR is CO_2. The strong positive spike in inorganic carbon concentrations and its absence in other sections of the core that are without negative $\delta^{34}S$ values supports the idea of active BSR.

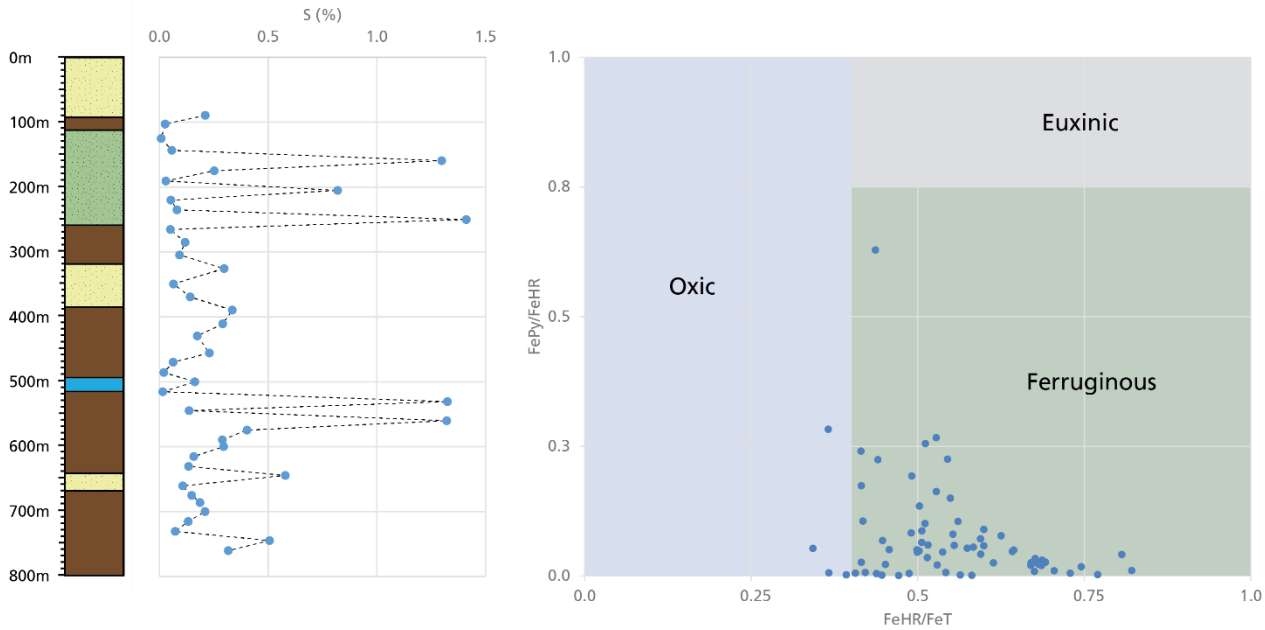

Figure 8: left: Variation in total sulphur concentrations in the Barb 5 drill core; right: cross-plot of FePy/FeHR (DOP) ratio vs. FeHR/FeT for shales from the Barb 5 drill core, modified after Raiswell and Canfield (2012)

An explanation of the negative iron isotope excursion is, however, less straight-forward. BSR produces large amounts of sulphides and inorganic carbon that could potentially react and withdraw light iron from the seawater. Due to their low solubility, sulphides react readily with iron to form pyrite or one of its precursors. Negative δ^{56}Fe values in pyrite have been interpreted to reflect either isotopically light seawater composition or fractionation during mineral formation (Johnson et al. 2008b). Yet, in the case of the Barb 5 core, iron-rich carbonates are particularly abundant in the volcanoclastic unit. Similar to pyrite, light iron isotopes are slightly enriched in iron carbonates. The experimentally determined values reported by Wiesli et al. (2004) indeed fall within the range of the observed values. In fact, Archean oceans likely contained sufficient iron to compensate for sulphide and CO_2 and to produce both pyrite and iron carbonates. Since total iron concentrations in the volcanoclastic unit were lower than in some underlying shales, and because sulphur concentrations increased in the same section, it is probable that a major fraction of iron was originally incorporated into pyrite. This agrees with the speculated secondary nature of carbonates (see discussion in 3.3.).

As discussed, diagenetic minerals like pyrite can reflect both a seawater signature and fractionation processes during their formation. While their influence cannot be quantified, considerations of the basin development and the depositional setting can help to compare the importance of respective processes in different parts of the core. With a reservoir depleted in heavy iron at the begin of Middle Mapepe times (see section 3.3. and Planavsky et al. (2012)), diagenetic minerals in the lowermost part of the Barb 5 core could have incorporated this light isotopic signature. Influence of new, terrestrial iron input (as discussed in 3.3.) increases during basin development and shifts the reservoir towards crustal isotopic signatures. Following the argumentation in section 3.3., partial Fe(II) oxidation also gains importance in shallower parts of the

basin and will partially counteract this development. Still, the most negative $\delta^{56}Fe$ values occurred in the volcanoclastic unit. If formation of diagenetic iron phases was rapid, and if burial was quick, a kinetic fractionation signature could have been preserved. Coarser grain sizes observed in the volcanoclastic part of the drill core indicate an environment with higher energies and more rapid deposition of sediment. Such environments do not inhibit circulation of pore fluids, but isotopic exchange with seawater is probably limited. Therefore it can be presumed that iron fractionation during mineral precipitation contributed more to the isotopic signature recorded in bulk rocks from the volcanoclastic unit than in bulk shales at the bottom of the drill core.

3.5 Depositional setting for organic carbon in the Archean – links between geochemistry and sedimentology

Observed total organic carbon concentrations of up to 2% in the lower part of the drill core are much higher than the average TOC contents in most Archean rocks. Significant amounts of organic carbon can only be preserved in the absence of remineralization mechanisms, including oxidation by free oxygen, DIR or BSR, as shown in modern sediments. In order to draw a coherent picture of the geochemical evolution of the Mapepe basin, understanding the conditions that allowed preservation is crucial. Contrary to the degree of remineralization in modern oceans, which depends on the time settling organic matter spends in the water column, suitable environments for preservation are preferably found in the deep anoxic Archean oceans. This conclusion confirms the sedimentological interpretation of the bottom of the Barb 5 drill core. The absence of terminal electron acceptors like Fe(III) or sulphate further indicates the lack of cycling of these elements. This is well illustrated by negative $\delta^{56}Fe$ at the drill core´s bottom that could be produced by iron cycling through DIR. On the other hand, DIR would oxidize organic carbon. Since both a light iron isotope signature and significant amounts of TOC are preserved, the bulk rock isotopic composition only reflects either seawater composition or fractionation during mineral precipitation (as discussed in 3.3. and 3.4.)

3.6 Mass balance

Many studies of iron isotopes, for instance in iron formations, show clusters of rocks with either heavier or lighter isotopic composition than the bulk crust. The majority of early Archean iron formations exhibits a heavy isotopic composition, whereas late Archean iron formations often show light isotope enrichment (Bekker et al. 2010). This also holds true for shales, though mass balance requires a balance of light and heavy isotopes. A mass weighted average of ~0‰ for the Barb 5 drill core was observed, which is close to the expected igneous crustal average of 0.09‰. In comparison to former studies, the high resolution analysis of the Mapepe basin better represents the range of fractionation processes in the Archean and the development of iron fractionation over time. Therefore, the results indicate that mass balance for other environments with stronger fractionation will be achieved if all pools of iron are integrated over sufficient time.

4. Conclusions

In conclusion, iron deposition in the Mapepe basin is likely not only controlled by weathering of older sequences and contemporaneous volcanic activity, but also by withdrawal of iron from the water column. A depositional model that can explain variation of iron isotopes involves five main sources of isotopically distinct iron: a) weathering of igneous rocks and contemporaneous volcanic activity that represent the crustal average ($\delta^{56}Fe \approx 0.1‰$), b) minor weathering of iron formations with positive $\delta^{56}Fe$, c) iron derived from anoxygenic photosynthetic iron oxidation with positive $\delta^{56}Fe$, d) a seawater source with a slightly light iron isotopic signature, and e) kinetic and equilibrium fractionation ($\delta^{56}Fe < 0$) during formation of iron-bearing minerals like pyrite or iron-carbonates.

In this model, the transformation of the basin from a deep anoxic environment, to a shallow, more active depositional setting governs iron deposition. In the beginning of early Mapepe deposition, iron was mainly derived from the water column and partially incorporated in pyrite that was in (near-) equilibrium with the seawater geochemistry. The redox environment was probably strongly reducing and iron was not actively cycled. Light bulk rock isotopic signatures represent mixing of mineral equilibria, particularly pyrite as shown by increased DOP values, and a light reservoir that was enriched in light isotopes during the formation of an underlying iron formation. In contrast, the top of the core represents a more active environment with rapid sedimentation and iron cycling. Positive $\delta^{56}Fe$ values represent a mixing of igneous source rocks and minor amounts of weathered iron formations with some preserved ferric iron minerals derived from enhanced anoxygenic photosynthesis in a shallower water column. Ferric iron minerals, most likely oxyhydroxides, were probably quickly altered during diagenesis or subsequent hydrothermal alteration, but possibly retained their isotopic signature. Trends in iron isotopes in bulk rock samples indicate a transition between these environments that is mainly determined by the topography of the depositional basin.

This transition is interrupted volcanic activity that leads to the deposition of a distinct unit within the Barb 5 core; this activity likely added sulphur to the basin which was then cycled. Partial reduction of sulphate caused negative sulphur isotopic signatures and the drawdown of iron from the seawater. The negative $\delta^{56}Fe$ values in bulk volcanoclastic rocks reflect a mixture of isotopically light seawater and kinetic fractionation during pyrite or carbonate formation.

Finally, this study shows that mass balance issues can be resolved with high resolution basinwide analysis.

5. Appendix

5.1 Sample preparation and digestion

PFA beakers used in this study were pre-cleaned by boiling in 1:1 concentrated pro-analysis grade (PA) HNO_3 and 1:1 concentrated PA HCl before further cleaning with 6-7 M double distilled (DD) HCl on a hotplate. Pipette tips were leached in 6-7 M DD HCl for several days and vials used for measurements were leached with 1% HNO_3. All materials were thoroughly rinsed with ultra-high-quality water derived from a Millipore apparatus before application. Only double distilled reagents were used for the chemical procedures.

Samples were provided as powders and were homogenized for 10-15 min with a mechanical shaker before separating a smaller ~0.5-1g fraction. Subsequently, sample fractions with ca. 300 µg iron were weighed and transferred into beakers under clean conditions. Their size was estimated with preliminary XRF iron concentration date. Typical amounts of powdered sample ranged between 2 and 6 mg, and maximum amounts were kept below 20 mg.

Sample digestion followed an adaptation of the method of (Dauphas et al. 2004; Dauphas et al. 2009b) who applied three digestion steps involving hydrofluoric acid, nitric acid, hydrochloric acid and hydrogen perchloride. Internal tests (Smeets & Galic, pers. comm., 2013) suggest that full digestion of the sample can be achieved in one step with elevated temperatures and extended boiling time (see Table 3: Digestion procedure and preparation for column extraction). In addition to the procedure of Dauphas et al., samples were oxidized two times to prevent loss of ferrous iron during column separation. To further inhibit any reduction of iron during subsequent steps, a small quantity of hydrogen peroxide was added to any six molar hydrochloric acid that was used for dissolution of the sample or elution of the matrix.

Table 3: Digestion procedure and preparation for column extraction

- **Digestion**: Addition of ~25 drops conc. HF, ~12 drops conc. HNO_3 and one drop conc. $HClO_4$
- Heating in closed beakers at 140°C for at least 24h
- **First Oxidation step**: Cooling down, evaporation for 2-3h at 120°C, cooling down and addition of 150 µl H_2O_2 (31%)
- Heat with closed lit at 120°C for 1h and evaporate at 150°C
- **Second Oxidation step**: Add two drops conc. HNO_3, one drop $HClO_4$ and 50 µl H_2O_2. Dry down at 150°C; Redissolve in 2 ml 6 M HCl + 0.001% H_2O_2

5.2 Column procedures

High precision and accurate analysis of iron isotopes relies on the absence of matrix and interfering elements that could hamper the isotopic analysis with a multi-collector inductively-coupled mass spectrometer (MC-ICPMS). Commonly, chemical separation protocols use anion-exchange resins to purify iron. In concentrated HCl, iron forms anion chloride-complexes that are strongly retained on the resin while matrix elements can be eluted. After elimination of the matrix, iron is eluted at lower HCl molarity (Dauphas et al. 2004). In this study, we adapted the separation protocol of (Dauphas et al. 2004; Dauphas et al. 2009b) and used Bio-Rad AG1-X8 200-400 mesh resin that was filled into Bio-Rad Poly-Prep Chromatography columns (Table 4).

Table 4: Column extraction

- **Column preparation**: Fill disposable Bio-Rad Poly-Prep polyethylene columns with 1 ml of AG1-X8 200-400 mesh Cl-form anion exchange resin
- **Precleaning sequence of resin**: 10 ml H_2O, 5 ml 1M HNO_3, 10 ml H_2O, 10 ml 0.4M HCl, 5 ml H_2O, 2 ml 6M HCl
- The resin is preconditioned with 3x 1 ml 6 M HCl + 0.001% H_2O_2
- Load 1-1.3 ml sample onto the column and dry down the rest
- **Elution of matrix**: **:** 1 ml 6M HCl + H_2O_2, repeat one time, 2 ml 6M HCl + H_2O_2, 4 ml 6M HCl + H_2O_2
- Change beakers to collect iron
- **Elution of Fe**: 3x 3 ml 0.4M HCl
- Evaporation at 120°C, reoxidation with two drops H_2O_2; the sample is left with closed lit for one hour and subsequently dried down at 120°C. Redissolution in 0.5 ml 6 M HCl + 0.001% H_2O_2
- The resin is suitable for a second re-use when precleaned with 10 ml 6-7 M HCl, 10 ml H_2O. If visibly dirty, the resin should be replaced. If needed, store columns were stored in 0.165 M HCl
- The column procedure is repeated a second time
- After drying down the sample, both the Fe fraction and the remainder of the digested sample were dissolved in 2 ml 1% HNO_3. The samples are now ready for analysis with ICP-OES and MC-ICPMS

Columns and resin were first cleaned with a sequence of H_2O, HNO_3 and HCl and the resin was preconditioned with 6 M HCl + 0.001% H_2O_2 (see Table 3). Then, 1-1.3 ml sample solution was loaded on the columns. After elution of the matrix with 8 ml 6 M HCl + 0.001% H_2O_2 within 4 steps, iron was eluted with 3x 3 ml 0.4 M HCl. Internal tests at the VU Amsterdam (Galic, pers. comm., 2013) confirmed that yields of 100 +/-2% can be obtained with this method. This purification procedure is very effective for most matrix elements including nickel and chromium, but some titanium is retained in the iron fraction. To ensure complete elimination of the matrix, the procedure was thus repeated before drying down both the iron fraction and the remainder of the digested sample and dissolving them in 2 ml 1% HNO_3.

5.3 ICP-OES analysis

In order to validate the column extraction procedure and to check for potential iron loss or isotope fractionation during purification (Anbar et al. 2000), the iron fraction was compared with the digested sample using a Varian 720-ES ICP-OES (see Table 5 for conditions and settings). Samples were acidified and diluted to concentrations between 2 and 4 ppm with 1% HNO_3. Total iron concentrations were determined at the 238.204 nm, 259.940 nm and 261.187 nm bands and are reported as averages (Appendix XY).

Table 5: Conditions for metal concentration measurements using the Varian 720-ES ICP-OES

Conditions sets		**Sample introduction**	
Power (kW)	1.30	Sample uptake (s)	40
Plasma flow (L/min)	15.0	Rinse time (s)	10
Auxiliary flow (L/min)	1.50	Pump rate (rpm)	15
Nebulizer flow (L/min)	0.75	**General settings**	
Replicate time (s)	10	Replicates	6
Stabilization time (s)	15		

Standards made from a 1000ppm Merck IV multi-element solution were prepared to calibrate the instrument and evaluate analytical accuracy and instrumental drift. The instrumental precision of total iron analysis for a set of six replicates was 2% (RSD) or better, typically around 1% (RSD). The errors of lab

instruments like variable pipettes exceed those of the instrument, therefore total analytical precision depends on sample preparation. During each set of samples measured on the ICP-OES, a small concentration depended drift of 0.1% - 0.3% between two samples was observed. However, since pairs of whole rock and purified sample were grouped together during the measurements, no drift correction has to be applied for the purpose of these analysis, that is, control of iron loss.

Despite a sufficient precision in between two measurements, comparison of concentrations before and after purification is not straight-forward due to matrix effects that influence ICP-OES analysis. The iron content of most samples apparently increased by ~2-5% during purification. Measurements of blanks that were also subject to the chemical procedure indeed show contamination with iron, but this contamination is negligible at <0.5‰ of the total amount of iron in the samples. Therefore, our results indicate that measured Fe concentrations decrease due to matrix effects, with the exception of rocks rich in organic matter (e.g. geological standard SGR-1). Since apparent iron enrichment was also observed for geological standards, similar results may be considered to represent a ~100% yield. Only samples B99, B56, B50, B41 and B36 exhibited stronger differences with ≤95% or ≥108% yield and should be treated carefully (see Appendix 5.5). Anbar et al. (2000) report strong fractionation and enrichment in heavy isotopes if iron is lost in the chromatographic column. With the exception of B41, iron in the samples of concern was lighter or in between relative to the values of their neighbouring samples. This indicates that observed deviations in concentrations are more likely from analytical inaccuracies, e.g. during the weighing of sample powders or pipetting. Thus, these samples may also be accepted for isotope analysis for the purpose of this study.

5.4 Mass-spectrometer set-up

Iron isotopes were measured on a ThermoFinnigan Neptune MC-ICPMS at the VU University Amsterdam (VUA), following the method suggested by Weyer, Schwieters (2003). Here, a combination of high mass resolution entrance and low mass resolution detector slits is used to achieve a high mass resolving power of about 8000-9000[4]. This ensures steep peak slopes and flat peak shapes that are necessary to separate iron from its isobaric polyatomic interferences like $^{40}Ar^{16}O^{+}$ on $^{56}Fe^{+}$ or $^{40}Ar^{14}N^{+}$ on $^{54}Fe^{+}$. All samples and standard solutions were diluted to approximately 1ppm Fe in 1% HNO_3 and were introduced with a Cetac Aridus desolvating nebulizer that was optimized for high sensitivity. We used a standard sample bracketing technique to monitor instrumental mass bias and calculate $\delta^{56}Fe$ values. Pure 1% HNO_3 blanks were measured before and after each standard and sample: for example, *Blank – Standard – Blank – Sample – Blank – Standard – Blank*. When evaluating the data, only values with a sufficiently strong signal (> 10kV), low blank levels (< 1 mV) and low drift (< 0.1‰) between the standard measurements were accepted. All iron isotope values are reported using the delta notation (Beard et al. 2003; Dauphas et al. 2004):

$$\partial^{56}Fe = \left(\frac{^{56}Fe / ^{54}Fe_{sample}}{^{56}Fe / ^{54}Fe_{IRMM-014}} - 1 \right) * 10^{3}$$

[4] Weyer and Schwieters (2003) define the resolving power of a MC-ICPMS as $R_{power}(5,95\%) = m / \Delta m$ with the peak height m and Δm^{*} indicating the difference between the mass at 5% of the peak height and 95% of the peak height.

The instrumental precision based on repeated measurements of an internal standard was ~0.16 ‰. We also processed international geological standards that yielded average $\delta^{56}Fe$ values of 0.10‰ for BHVO-2, 0.09‰ for MAG-1 and 0.045‰ for SGR-1. These results compare well with other published values within the range of error (e.g. Craddock, Dauphas 2011; Wang et al. 2012; Beard et al. 2003; Dideriksen et al. 2006; see table 2). However, no external precision can be given here due to the low number of measurements.

5.5 Data

Sample No.	B-number	Rock type	average depth [m]	Fe_2O_3	difference Fe content after column procedure	δ56 preliminary	S(%)	TIC	TOC
BARB5-089.44	**133**	Sandstone	89.52	3.5	4.2	0.17	0.21	0.09	0.46
BARB5-102.68	**130**	Sandstone	102.77	15.9	2.7	-0.09	0.03	9.31	0.99
BARB5-125.06	**126**	Volcaniclastic rock	125.14	3.3	-0.2	0.32	0.01	0.89	0.42
BARB5-143.28	**123**	Chert	143.36	1.2	3.0	0.34	0.06	0.56	0.20
BARB5-159.20	**120**	Volcaniclastic rock	159.28	1.1	5.3	0.04	1.30	0.43	0.38
BARB5-174.75	**117**	Volcaniclastic rock	174.84	14.2	3.7	-0.12	0.25	7.71	1.40
BARB5-190.60	**114**	Volcaniclastic rock	190.69	0.9	2.3	0.16	0.03	0.53	0.20
BARB5-205.17	**111**	Sandy shale	205.25	1.1	4.1	-0.03	0.82	0.61	0.31
BARB5-220.03	**108**	Sandstone	220.13	11.7	-0.4	-0.40	0.05	7.35	0.85
BARB5-235.12	**105**	Volcaniclastic rock	235.20	4.7	2.1	-0.10	0.08	2.84	0.52
BARB5-250.07	**102**	Volcaniclastic rock	250.15	0.5	-2.3	-0.46	1.41	0.39	0.22
BARB5-265.30	**99**	Sandy shale	265.39	4.9	8.3	-0.08	0.05	1.83	0.57
BARB5-285.04	**95**	Carbonaceous shale	285.14	5.1	1.7	0.04	0.12	0.86	0.63
BARB5-304.77	**91**	Carbonaceous shale	304.85	10.9	2.9	0.42	0.09	1.81	0.84
BARB5-325.60	**87**	Conglomerate	325.70	3.2	3.7	-0.03	0.30	0.59	0.67
BARB5-349.44	**83**	Conglomerate	349.52	1.8	5.6	-0.05	0.06	1.26	0.41
BARB5-369.07	**79**	Conglomerate	369.16	2.7	3.8	0.11	0.14	2.53	0.47
BARB5-389.52	**75**	Carbonaceous shale	389.59	20.8	-0.2	0.31	0.33	4.16	1.50
BARB5-410.55	**71**	Carbonaceous shale	410.63	11.2	7.7	-0.11	0.29	2.89	1.33
BARB5-429.38	**67**	Carbonaceous shale	429.46	20.3	-4.2	-0.29	0.17	1.10	3.26
BARB5-455.63	**62**	Carbonaceous shale	455.73	13.0	5.8	-0.03	0.23	2.23	1.77
BARB5-469.70	**59**	Carbonaceous shale	469.79	13.2	3.3	0.15	0.06	2.12	1.27
BARB5-485.47	**56**	Carbonaceous shale	485.56	20.5	9.2	-0.29	0.02	2.62	0.55
BARB5-500.10	**53**	Shale	500.19	36.0	1.6	0.15	0.16	4.30	0.71
BARB5-515.33	**50**	Carbonaceous shale	515.41	10.0	-5.1	-0.14	0.01	1.46	0.59
BARB5-530.45	**47**	Carbonaceous shale	530.53	11.1	-3.1	0.13	1.32	1.05	0.87

Sample No.	B-number	Rock type	average depth [m]	Fe_2O_3	difference Fe content after column procedure	δ56 preliminary	S(%)	TIC	TOC
BARB5-544.36	**44**	Carbonaceous shale	544.45	12.2	1.3	-0.06	0.14	1.22	0.97
BARB5-560.00	**41**	Carbonaceous shale	560.08	15.0	33.2	0.34	1.32	1.63	0.95
BARB5-574.56	**38'**	Carbonaceous shale	574.65	15.0	6.0	0.12	0.40	0.98	1.46
BARB5-589.41	**36**	Carbonaceous shale	589.47	11.1	-9.2	-0.12	0.29	1.03	0.95
BARB5-599.83	**33**	Carbonaceous shale	599.91	12.6	2.1	-0.02	0.30	1.33	1.10
BARB5-615.03	**30**	Carbonaceous shale	615.11	8.7	1.3	-0.07	0.16	0.78	1.33
BARB5-630.43	**27**	Carbonaceous shale	630.51	11.0	0.5	-0.15	0.13	2.33	1.34
BARB5-644.24	**24**	Carbonaceous shale	644.33	10.2	-1.5	-0.25	0.58	1.15	1.25
BARB5-660.40	**21**	Carbonaceous shale	660.48	8.0	2.2	-0.18	0.11	0.53	1.21
BARB5-675.22	**18**	Carbonaceous shale	675.30	6.4	1.1	-0.13	0.15	0.40	1.97
BARB5-686.13	**15'**	Carbonaceous shale	686.20	8.8	0.3	-0.09	0.19	0.71	0.90
BARB5-700.01	**13**	Carbonaceous shale	700.09	9.4	-1.4	-0.01	0.21	0.94	1.16
BARB5-715.21	**10**	Carbonaceous shale	715.31	10.6	-3.9	-0.15	0.13	0.76	2.05
BARB5-730.51	**7**	Shale	730.58	11.7	1.4	-0.17	0.07	0.72	1.83
BARB5-744.74	**4**	Carbonaceous shale	744.82	9.4	-3.8	0.10	0.51	0.88	1.78
BARB5-760.15	**1**	Carbonaceous shale	760.23	12.7	1.4	-0.16	0.32	1.20	1.99

Acknowledgements

I want to thank Aleksandra Galic, Paul Mason and Pieter Vroon for helping to organize this project. Their guidance and constructive input significantly improved this work – next to getting me thinking. Thank you also to Richard Smeets, Bas van der Waagt and John Visser for their tremendous help with analytical procedures and their patience during numerous explanations.

The analytical part of this research was funded by the Netherlands Organisation for Scientific Research (NWO).

Publication bibliography

Albarede, F. (1998): The growth of continental crust. In *Tectonophysics* 296 (1-2), pp. 1–14.

Anbar, A. D. (2004): Iron stable isotopes: Beyond biosignatures. In *Earth and Planetary Science Letters* 217 (3-4), pp. 223–236.

Anbar, A. D.; Roe, J. E.; Barling, J.; Nealson, K. H. (2000): Nonbiological fractionation of iron isotopes. In *Science* 288 (5463), pp. 126–128.

Anbar, A. D.; Rouxel, O. J. (2007): Metal stable isotopes in paleoceanography. In *Annual Review of Earth and Planetary Sciences* 35, pp. 717–746.

Armstrong, R. L. (1981): Radiogenic isotopes - the case for crustal recycling on a near-steady-state no-continental-growth earth. In *Philosophical Transactions of the Royal Society A-Mathematical, Physical and Engineering Sciences* 301 (1461), pp. 443–472.

Arndt, N. T.; Nisbet, E. G. (2012): Processes on the young earth and the habitats of early life. In R. Jeanloz (Ed.): Annual Review of Earth and Planetary Sciences, vol. 40. Palo Alto, USA: Annual Reviews (Annual Review of Earth and Planetary Sciences), pp. 521–549.

Bau, M. (1991): Rare-earth element mobility during hydrothermal and metamorphic fluid rock interaction and the significance of the oxidation-state of europium. In *Chemical Geology* 93 (3-4), pp. 219–230.

Beard, B. L.; Johnson, C. M. (2004): Fe isotope variations in the modern and ancient earth and other planetary bodies. In C. M. Johnson, B. L. Beard, F. Albarede (Eds.): Geochemistry of non-traditional stable isotopes, vol. 55. AGU CGU. Chantilly, USA: Mineralogical Society of America (Reviews in Mineralogy & Geochemistry), pp. 319–357.

Beard, B. L.; Johnson, C. M.; Cox, L.; Sun, H.; Nealson, K. H.; Aguilar, C. (1999): Iron isotope biosignatures. In *Science* 285 (5435), pp. 1889–1892.

Beard, B. L.; Johnson, C. M.; Skulan, J. L.; Nealson, K. H.; Cox, L.; Sun, H. (2003): Application of Fe isotopes to tracing the geochemical and biological cycling of Fe. In *Chemical Geology* 195 (1-4), pp. 87–117.

Bekker, A.; Holland, H. D.; Wang, P. L.; Rumble, D.; Stein, H. J.; Hannah, J. L. et al. (2004): Dating the rise of atmospheric oxygen. In *Nature* 427 (6970), pp. 117–120.

Bekker, A.; Slack, J. F.; Planavsky, N.; Krapez, B.; Hofmann, A.; Konhauser, K. O.; Rouxel, O. J. (2010): Iron formation: The sedimentary product of a complex interplay among mantle, tectonic, oceanic, and biospheric processes. In *Economic Geology* 105 (3, SI), pp. 467–508.

Bigeleisen, J. (1965): Chemistry of isotopes. In *Science* 147 (3657), pp. 463–471.

Bontognali, T. R. R.; Fischer, W. W.; Föllmi, K. B. (2013): Siliciclastic associated banded iron formation from the 3.2Ga Moodies Group, Barberton Greenstone Belt, South Africa. In *Precambrian Research* 226, pp. 116–124.

Buick, R. (2008): When did oxygenic photosynthesis evolve? In *Philosophical Transactions of the Royal Society B-Biological Sciences* 363 (1504), pp. 2731–2743.

Bullen, T. D.; White, A. F.; Childs, C. W.; Vivit, D. V.; Schulz, M. S. (2001): Demonstration of significant abiotic iron isotope fractionation in nature. In *Geology* 29 (8), pp. 699–702.

Butler, I. B.; Archer, C.; Vance, D.; Oldroyd, A.; Rickard, D. (2005): Fe isotope fractionation on FeS formation in ambient aqueous solution. In *Earth and Planetary Science Letters* 236 (1-2), pp. 430–442.

Canfield, D. E. (2001): Biogeochemistry of sulfur isotopes. In : Stable isotope geochemistry, vol. 43. WASHINGTON DC, USA: Mineralogical Society of America (Reviews in Mineralogy & Geochemistry), pp. 607–636.

Canfield, D. E. (2005): The early history of atmospheric oxygen: Homage to Robert A. Garrels. In *Annual Review of Earth and Planetary Sciences* 33, pp. 1–36.

Craddock, P. R.; Dauphas, N. (2011): Iron isotopic compositions of geological reference materials and chondrites. In *Geostandards and Geoanalytical Research* 35 (1), pp. 101–123.

Croal, L. R.; Johnson, C. M.; Beard, B. L.; Newman, D. K. (2004): Iron isotope fractionation by Fe(II)-oxidizing photoautotrophic bacteria. In *Geochimica et Cosmochimica Acta* 68 (6), pp. 1227–1242.

Dauphas, N.; Craddock, P. R.; Asimov, P. D.; Bennett, V. C.; Nutman, A. P.; Ohnenstetter, D. (2009a): Iron isotopes may reveal the redox conditions of mantle melting from Archean to Present. In *Earth and Planetary Science Letters* 288 (1-2), pp. 255–267.

Dauphas, N.; Janney, P. E.; Mendybaev, R. A.; Wadhwa, M.; Richter, F. M.; Davis, A. M. et al. (2004): Chromatographic Separation and Multicollection-ICPMS Analysis of Iron. Investigating Mass-Dependent and -Independent Isotope Effects. In *Anal. Chem.* 76 (19), pp. 5855–5863.

Dauphas, N.; Pourmand, A.; Teng, F.-Z. (2009b): Routine isotopic analysis of iron by HR-MC-ICPMS: How precise and how accurate? In *Chemical Geology* 267 (3-4), pp. 175–184.

Dauphas, N.; Rouxel, O. J. (2006): Mass spectrometry and natural variations of iron isotopes. In *Mass Spectrometry Reviews* 25 (4), pp. 515–550.

Dideriksen, K.; Baker, J. A.; Stipp, S.L.S. (2006): Iron isotopes in natural carbonate minerals determined by MC-ICP-MS with a 58Fe–54Fe double spike. In *Geochimica et Cosmochimica Acta* 70 (1), pp. 118–132.

Farquhar, J.; Peters, M.; Johnston, D. T.; Strauss, H.; Masterson, A.; Wiechert, U.; Kaufman, A. J. (2007): Isotopic evidence for Mesoarchaean anoxia and changing atmospheric sulphur chemistry. In *Nature* 449 (7163), pp. 706-U5.

Farquhar, J.; Wing, B. A. (2003): Multiple sulfur isotopes and the evolution of the atmosphere. In *Earth and Planetary Science Letters* 213 (1-2), pp. 1–13.

Flament, N.; Coltice, N.; Rey, P. F. (2008): A case for late-Archaean continental emergence from thermal evolution models and hypsometry. In *Earth and Planetary Science Letters* 275 (3-4), pp. 326–336.

Grassineau, N. V.; Abell, P.; Appel, P. W. U.; Lowry, D.; Nisbet, E. G. (2006): Early life signatures in sulfur and carbon isotopes from Isua, Barberton, Wabigoon (Steep Rock), and Belingwe Greenstone Belts (3.8 to 2.7 Ga). In : Memoir 198: Evolution of early earth's atmosphere, hydrosphere, and biosphere - constraints from ore deposits, vol. 198: Geological Society of America, pp. 33–52.

Hofmann, A. (2005): The geochemistry of sedimentary rocks from the Fig Tree Group, Barberton greenstone belt: Implications for tectonic, hydrothermal and surface processes during mid-Archaean times. In *Precambrian Research* 143 (1-4), pp. 23–49.

Hofmann, A.; Harris, C. (2008): Silica alteration zones in the Barberton greenstone belt: A window into subseafloor processes 3.5–3.3 Ga ago. In *Chemical Geology* 257 (3-4), pp. 221–239.

Icopini, G. A.; Anbar, A. D.; Ruebush, S. S.; Tien, M.; Brantley, S. L. (2004): Iron isotope fractionation during microbial reduction of iron: The importance of adsorption. In *Geology* 32 (3), pp. 205–208.

Johnson, C. M.; Beard, B. L.; Klein, C.; Beukes, N. J.; Roden, E. E. (2008a): Iron isotopes constrain biologic and abiologic processes in banded iron formation genesis. In *Geochimica et Cosmochimica Acta* 72 (1), pp. 151–169.

Johnson, C. M.; Beard, B. L.; Roden, E. E. (2008b): The iron isotope fingerprints of redox and biogeochemical cycling in the modern and ancient Earth. In *Annual Review of Earth and Planetary Sciences* 36, pp. 457–493.

Kasting, J. (1993): Earth's early atmosphere. In *Science* 259 (5097), pp. 920–926.

Krüner, A.; Byerly, G. R.; Lowe, D. R. (1991): Chronology of early Archean granite-greenstone evolution in the Barberton Mountain Land, South Africa, based on precise dating by single zircon evaporation. In *Earth and Planetary Science Letters* 103 (1-4), pp. 41–54.

Lowe, D. R.; Byerly, G. R. (1999): Stratigraphy of the west-central part of the Barberton Greenstone Belt, South Africa. In : Special Paper 329: Geologic evolution of the Barberton Greenstone Belt, South Africa, vol. 329: Geological Society of America, pp. 1–36.

Lowe, D. R.; Byerly, G. R. (2007): Ironstone bodies of the Barberton greenstone belt, South Africa: Products of a Cenozoic hydrological system, not Archean hydrothermal vents! In *Geological Society of America Bulletin* 119 (1-2), pp. 65–87.

Lowe, D. R.; Nocita, B. W. (1999): Foreland basin sedimentation in the Mapepe Formation, southern-facies Fig Tree Group. In : Special Paper 329: Geologic evolution of the Barberton Greenstone Belt, South Africa, vol. 329: Geological Society of America, pp. 233–258.

Michard, A.; Albarede, F. (1986): The Ree content of some hydrothermal fluids. In *Chemical Geology* 55 (1-2), pp. 51–60.

Ohmoto, H.; Watanabe, Y.; Yamaguchi, K. E.; Naraoka, H.; Haruna, M.; Kakegawa, T. et al. (2006): Chemical and biological evolution of early Earth: Constraints from banded iron formations. In : Memoir 198: Evolution of early earth's atmosphere, hydrosphere, and biosphere - constraints from ore deposits, vol. 198: Geological Society of America, pp. 291–331.

Planavsky, N.; Bekker, A.; Rouxel, O. J.; Kamber, B. S.; Hofmann, A.; Knudsen, A.; Lyons, T. W. (2010): Rare Earth Element and yttrium compositions of Archean and Paleoproterozoic Fe formations revisited: New perspectives on the significance and mechanisms of deposition. In *Geochimica et Cosmochimica Acta* 74 (22), pp. 6387–6405.

Planavsky, N.; Rouxel, O. J.; Bekker, A.; Hofmann, A.; Little, C. T. S.; Lyons, T. W. (2012): Iron isotope composition of some Archean and Proterozoic iron formations. In *Geochimica et Cosmochimica Acta* 80, pp. 158–169.

Poulton, S. W.; Canfield, D. E. (2005): Development of a sequential extraction procedure for iron: implications for iron partitioning in continentally derived particulates. In *Chemical Geology* 214 (3-4), pp. 209–221.

Poulton, S. W.; Krom, M. D.; Raiswell, R. (2004): A revised scheme for the reactivity of iron (oxyhydr)oxide minerals towards dissolved sulfide. In *Geochimica et Cosmochimica Acta* 68 (18), pp. 3703–3715.

Raiswell, R.; Canfield, D. E. (2012): The iron biogeochemical cycle past and present. In *GeochemPersp* 1 (1), pp. 1–220.

Rosing, M. T. (1999): 13C-depleted carbon microparticles in >3700-Ma sea-floor sedimentary rocks from West Greenland. In *Science* 283 (5402), pp. 674–676.

Rouchon, V.; Orberger, B.; Hofmann, A.; Pinti, D. L. (2009): Diagenetic Fe-carbonates in Paleoarchean felsic sedimentary rocks (Hooggenoeg Formation, Barberton greenstone belt, South Africa): Implications for CO2 sequestration and the chemical budget of seawater. In *Precambrian Research* 172 (3-4), pp. 255–278.

Schauble, E. A. (2004): Applying stable isotope fractionation theory to new systems. In C. M. Johnson, B. L. Beard, F. Albarede (Eds.): Geochemistry of non-traditional stable isotopes, vol. 55. AGU CGU. Chantilly, USA: Mineralogical Society of America (Reviews in Mineralogy & Geochemistry), pp. 65–111.

Taylor, S. R.; McLennan, S. M. (1985): The continental crust: Its composition and evolution. An examination of the geochemical record preserved in sedimentary rocks. Oxford: Blackwell Scienctific.

Tice, M. M.; Lowe, D. R. (2004): Photosynthetic microbial mats in the 3,416-Myr-old ocean. In *Nature* 431 (7008), pp. 549–552.

Valley, J. W.; Cavosie, A. J.; Ushikubo, T.; Reinhard, D. A.; Lawrence, D. F.; Larson, D. J. et al. (2014): Hadean age for a post-magma-ocean zircon confirmed by atom-probe tomography. In *Nature Geosci*.

Van Kranendonk, M. J.; Webb, G. E.; Kamber, B. S. (2003): Geological and trace element evidence for a marine sedimentary environment of deposition and biogenicity of 3.45 Ga stromatolitic carbonates in the Pilbara Craton, and support for a reducing Archaean ocean. In *Geobiology* 1 (2), pp. 91–108.

Wang, K.; Moynier, F.; Dauphas, N.; Barrat, J.; Craddock, P. R.; Sio, C. K. (2012): Iron isotope fractionation in planetary crusts. In *Geochimica et Cosmochimica Acta* 89, pp. 31–45.

Weyer, S.; Schwieters, J.B (2003): High precision Fe isotope measurements with high mass resolution MC-ICPMS. In *International Journal of Mass Spectrometry* 226 (3), pp. 355–368.

Wiesli, R. A.; Beard, B. L.; Johnson, C. M. (2004): Experimental determination of Fe isotope fractionation between aqueous Fe(II), siderite and "green rust" in abiotic systems. In *Chemical Geology* 211 (3-4), pp. 343–362.

Wilde, S. A.; Valley, J. W.; Peck, W. H.; Graham, C. M. (2001): Evidence from detrital zircons for the existence of continental crust and oceans on the Earth 4.4 Gyr ago. In *Nature* 409 (6817), pp. 175–178.

Yamaguchi, K. E.; Johnson, C. M.; Beard, B. L.; Ohmoto, H. (2005): Biogeochemical cycling of iron in the Archean-Paleoproterozoic Earth: Constraints from iron isotope variations in sedimentary rocks from the Kaapvaal and Pilbara Cratons. In *Chemical Geology* 218 (1-2), pp. 135–169.